Research Article | Vol. 24, No. 23 | 14 Nov 2016 | OPTICS EXPRESS 26503
Optics EXPRESS

Maximization of the optical intra-cavity power of whispering-gallery mode resonators via coupling prism

G. A. Santamaría-Botello,[1] L. E. García Muñoz,[1,*] F. Sedlmeir,[2] S. Preu,[3] D. Segovia-Vargas,[1] K. Atia Abdalmalak,[1] S. Llorente Romano,[1] A. García Lampérez,[1] S. Malzer,[4] G. H. Döhler,[4] H. G. L. Schwefel,[2] and H. B. Weber[4]

[1]*Dpto. de Teoría de la señal y Comunicaciones. Universidad Carlos III de Madrid, Leganés, Spain*
[2]*The Dodd-Walls Centre for Photonic and Quantum Technologies, Department of Physics, University of Otago, Dunedin, New Zealand*
[3]*Technical University of Darmstadt, Germany*
[4]*Lehrstuhl für Angewandte Physik, Universität Erlangen-Nürnberg, Germany*
[*]*legarcia@ing.uc3m.es*

Abstract: In this paper, a detailed description of the optical coupling into a Whispering Gallery Mode (WGM) resonator through a prism via frustrated total internal reflection (FTIR) is presented. The problem is modeled as three media with planar interfaces and closed expressions for FTIR are given. Then, the curvature of the resonator is taken into account and the mode overlap is theoretically studied. A new analytical expression giving the optimal geometry of a disc-shaped or ring-shaped resonator for maximizing the intra-cavity circulating power is presented. Such expression takes into consideration the spatial distribution of the WGM at the surface of the resonator, thus being more accurate than the currently used expressions. It also takes into account the geometry of the prism. It is shown an improvement in the geometry values used with the current expressions of about 30%. The reason why the pump laser signal can be seen in experiments under critical coupling is explained on this basis. Then, the conditions required for exciting the highest possible optical power inside the resonator are obtained. The aim is to achieve a highly-efficient up-conversion of a THz signal into the optical domain via the second-order nonlinearity of the resonator material.

OCIS codes: (230.0230) Optical devices; (260.0260) Physical optics.

References and links

1. JPL, "BICEP2. II. Experiment and three-year data set," Astrophys. J. **792**(1), 62 (2014).
2. G. Carpintero, E. G. Muñoz, H. Hartnagel, S. Preu, A. Raisanen, *Semiconductor TeraHertz Technology: Devices and Systems at Room Temperature Operation* (Wiley-IEEE Press, 2015).
3. B. S. Karasik, and A. V. Sergeev, "THz Hot-Electron Photon Counter," IEEE Trans. Appl. Superconductivity **15**(2), 618–621 (2005).
4. D.V. Strekalov, A. A. Savchenkov, A. B. Matsko and N. Yu, "Towards Counting microwave photons at room temperature," Laser Phys. Lett. **6**(2), 129–134 (2009).
5. A. B. Shehata, C. Scarcella and A. Tosi, "Photon counting module based on InGaAs/InP Single-Photon Avalanche Diodes for near-infrared counting up to 1.7 Âţm," in *Ph.D. Research in Microelectronics and Electronics (PRIME), 2011 7th Conference on*, 177–180 (2011).
6. R. W. Boyd, *Nonlinear Optics* (Academic Press, 2003).
7. A. Rueda, F. Sedlmeir, M. C. Collodo, U. Vogl, B. Stiller, G. Schunk, D. V. Strekalov, C. Marquardt, J. M. Fink, O. Painter, G. Leuchs, and H. G. L. Schwefel, "Efficient microwave to optical photon conversion: an electro-optical realization," Optica **3**(6), 597–604 (2016).
8. D. V. Strekalov, C. Marquardt, A. B. Matsko, H. G. L. Schwefel, and G. Leuchs, "Nonlinear and Quantum Optics with Whispering Gallery Resonators," arXiv:1605.07972 [physics, Physics:quant-Ph] (2016).
9. F. Sedlmeir, M. R. Foreman, U. Vogl, R. Zeltner, G. Schunk, D. V. Strekalov, C. Marquardt, G. Leuchs, and H. G. L. Schwefel, "Polarization-selective out-coupling of whispering gallery modes," arXiv:1608.07660 [physics] (2016).
10. P.E. Powers., *Fundamentals of Nonlinear Optics* (CRC Press, 2011).

#273467 http://dx.doi.org/10.1364/OE.24.026503
Journal © 2016 Received 7 Sep 2016; revised 26 Oct 2016; accepted 26 Oct 2016; published 8 Nov 2016

Optics EXPRESS

11. M. R. Foreman, F. Sedlmeir, H. G. L. Schwefel, and G. Leuchs, "Dielectric tuning and coupling of whispering gallery modes using an anisotropic prism," J. Opt. Soc. Am. B 33, 2177–2195 (2016).
12. M. L. Gorodetsky, and V. S. Ilchenko, "Optical Microsphere Resonators: Optimal Coupling to High-Q Whispering-Gallery Modes," J. Opt. Soc. Am. B **16**(1) 147–154 (1999).
13. A. N. Oraevsky, "Whispering-Gallery waves," Quantum Electron. **32**(5), 377–400 (2002).
14. B.E. Little, J. P. Laine, and H. A. Haus, "Analytic theory of coupling from tapered fibers and half-blocks into microsphere resonators," J. Lightwave Technol. **17**(4), 704–715 (1999).
15. A. Yariv., "Universal relations for coupling of optical power between microresonators and dielectric waveguides," Electron. Lett. **36**(4), 321–322 (2000).
16. I. Breunig, B. Sturman, F. Sedlmeir, H. G. L. Schwefel, and K. Buse, "Whispering gallery modes at the rim of an axisymmetric optical resonator: Analytical versus numerical description and comparison with experiment," Opt. Express **21**(25), 30683–30692 (2013).
17. D. V. Strekalov, A. A. Savchenkov, A. B. Matsko, N. Yu, "Efficient upconversion of sub-THz radiation in a high-Q whispering gallery resonator," Opt. Lett. **34**(6), 713–715 (2009).

1. Introduction

Currently the technological solutions for filling the so-called "THz gap" and detecting THz radiation are limited. Some applications require receivers with extremely high sensitivity able to detect (count) individual photons at THz and sub-THz frequencies. An example of high interest in cosmology is the indirect detection of primordial gravitational waves by measuring the B-mode polarization of the cosmic microwave background (CMB) [1]. Semiconductor detector technology has however not reached the photon-counting limit at room temperature [2]. Indeed, photon counting THz and sub-THz receivers available to date operate under cryogenic conditions, which makes them expensive and difficult to implement [3].

Another approach in the pursuit of a room-temperature photon-counting THz receiver is nonlinear parametric up-conversion of the THz radiation into the optical domain [4], where photons are more energetic and photon counting detectors working at room temperature (for example, avalanche diodes) are currently available [5]. In this approach, a laser optical field (pump) at frequency ω_p is mixed with the THz radiation at frequency ω_m inside a second-order $\chi^{(2)}$ nonlinear dielectric to produce sidebands at frequencies $\omega_{s+} = \omega_p + \omega_m$ and $\omega_{s-} = \omega_p - \omega_m$, corresponding to sum-frequency-generation (SFG) and difference-frequency-generation (DFG) respectively [6]. The efficiency of the nonlinear up-conversion which is defined as the ratio of the output sideband power to input THz power, increases with the input optical power, the length of the interaction path, and the nonlinear $\chi^{(2)}$ interaction tensor [7]. This makes whispering gallery mode (WGM) resonators made of nonlinear crystals suitable for these applications since their circular-shaped geometry guides the field along the border so it continuously interferes constructively with itself after each round-trip, resulting in a circulating WGM with a power in steady-state several times higher than the incoming power [8]. As the guiding mechanism is purely governed by the geometry of the resonator, another WGM within the transparency region of the crystal with similar modal profile can be also excited. If such mode (for example the THz field) has the same phase velocity in every point as the optical WGM, a phase-matched [10] and thus efficient up-conversion of the THz signal takes place.

Usually, both WGMs are excited by near-field coupling [11]. For the optical WGM, the evanescent field arising from a prism surface when a laser beam is incident beyond the critical angle is commonly used [12]. The way the optical field is optimally coupled into the WGM resonator is the main topic discussed in this work. We will focus on deriving analytical expressions for the optical coupling through a prism under total internal reflection in order to optimize the intra-cavity circulating power. For this, the optimal gap between prism and resonator will be found by means of a plane waves model, whereas the optimal geometry of the resonator will be obtained by taking into account the spatial field distribution of both, the optical Gaussian beam refracted inside the prism and the WGM at the surface of the resonator. The paper is structured as follows: In Section 2 we model the coupling mechanism as three dielectric layers with planar

Optics EXPRESS

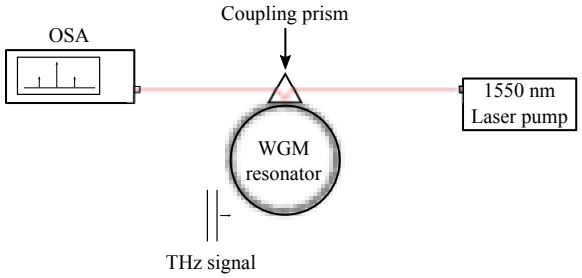

Fig. 1. Nonlinear up-conversion THz receiver. The laser beam is incident into the coupling prism and an optic WGM is excited in the resonator. By exciting another WGM for the THz signal the nonlinear interaction takes place and the up-converted signal is coupled out to the prism and detected by an optical spectrum analyzer.

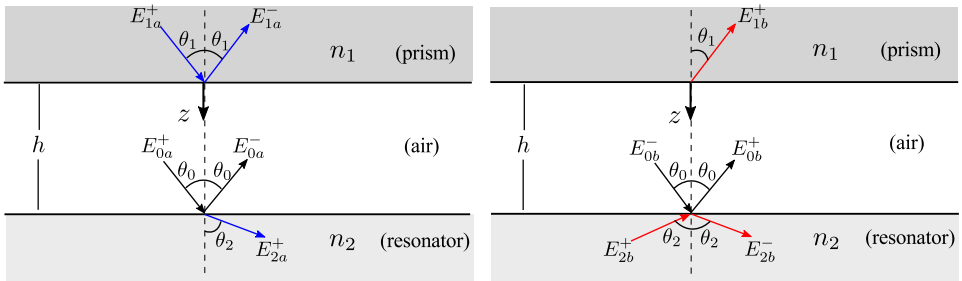

Fig. 2. Three media propagation model. n_1 and n_2 are the indices of refraction of the prism and resonator respectively. (a) Propagation from the prism. E_{1a}^{+} and E_{1a}^{-} are the incident and reflected electric fields evaluated in the prism-air interface respectively, whereas E_{2a}^{+} is the transmitted electric field evaluated in the air-resonator interface. (b) Propagation from the resonator. E_{2b}^{+} and E_{2b}^{-} are the incident and reflected electric fields evaluated in the resonator-air interface respectively, whereas E_{1b}^{+} is the transmitted electric field evaluated in the air-prism interface.

interfaces, and derive the electromagnetic transmission and reflection coefficients. In Section 3 the conditions these coefficients must fulfill to maximize the field inside the WGM resonator are obtained. Then, in Section 4 the practical aspects of optimal coupling achievement are discussed. In Section 5, the resonator's curvature is considered and the optimal geometry is found in order to couple most of the laser's power. Finally, conclusions are given.

2. Optical coupling through prism

The general setup for a THz receiver based on nonlinear up-conversion inside a WGM resonator is shown in Fig. 1. The nonlinear interaction takes place in a disc-shaped or torus-shaped resonator made of a nonlinear material such as lithium niobate ($LiNbO_3$). The laser beam is incident onto a prism and coupled into the resonator via frustrated total internal reflection (FTIR). If optimal coupling is achieved, no power will be reflected back to the prism at the laser frequency as will be shown later. In this case, only the up-converted signal can couple out through the prism and then be detected by an optical detector [9]. All power delivered by the laser is trapped within the resonator, being partially lost by the radiation and intrinsic losses of the material, and partially used in the up-conversion. This way, the maximum possible level of optical field inside the resonator is accomplished.

Optics EXPRESS

The coupling region is formed by three nonmagnetic and isotropic dielectric media: prism-air-resonator. Even though nonlinear crystals such as $LiNbO_3$ are not isotropic, we only consider linearly polarized fields in one of the principal axes of the crystal [10]. This is permissible as commonly only one polarization component of the field will dominate the interaction. The full analytical solution of the coupling problem requires to solve the Helmholtz equation in the three media and then ensure the continuity of the tangential components of the fields. Due to the differences in the geometries involved, this problem is hard to solve and can instead be addressed by finding separately the WGM field distribution from the Helmholtz equation solution for the isolated resonator, and the evanescent field at the surface of an isolated prism. These fields are expanded in modes and the matching between them is studied yielding to an approximated solution of the problem [13]. Another approximated approach is to consider either the prism's evanescent field or the resonator's WGM field as a primary field source ignoring the presence of the other medium. From the primary field considered, the scattering in the other medium is studied. In this section, we make a different approximation and consider all media interaction by modeling the region as two planar interfaces between the three media and plane waves excitation as shown in Fig. 2(a). This is a good approximation for Fresnel's coefficients calculation since in our practical application the optical wavelengths are very short compared with the actual curvature radii of the interfaces. However, in order to consider spatial mode matching, the variation of the air thickness due to a slight curvature in the air-resonator interface, will be taken into account in the last section.

The solution of the Helmholtz equation inside the resonator shows that the WGM field travels partially outside the resonator as an evanescent field [14]. Hence, it is necessary to introduce an effective index of refraction n_{eff} of the resonator's material in order to calculate the phase velocity of the WGM at the rim of the resonator as c/n_{eff}, with c being the speed of light in vacuum. Due to the high confinement of optical WGMs, $n_{\text{eff}} \approx n_2$ for optical frequencies, where n_2 is the index of refraction of the resonator. Therefore, the evanescent field that must exist in the air gap in order to excite the WGM must have a wave vector projection on the surface of the prism equal to:

$$\kappa_{\text{wgm}} = \frac{\omega}{c} n_{\text{eff}} \approx \frac{\omega}{c} n_2 \tag{1}$$

where ω is the angular frequency. In the three planar media picture, the parallel-to-prism component of the wave vector is related to the incidence angle of the incoming wave θ_1 (see Fig. 2) as $\kappa_{||} = \frac{\omega}{c} n_1 \sin\theta_1$, which must match with κ_{wgm}, hence

$$\sin\theta_1 = \frac{n_{\text{eff}}}{n_1} \approx \frac{n_2}{n_1} \tag{2}$$

where n_1 is the refractive index of the prism. This can only be achieved if the refractive index of the prism is greater than the refractive index of the resonator. Therefore, the angle of incidence exceeds the critical angle between prism and air $\theta_{c1} = \arcsin(n_0/n_1)$, and the expected evanescent field is created in the air gap.

Regarding the propagation process in the three media for arbitrary incidence angle θ_1 and electric field polarized perpendicularly to the plane of incidence, at the prism-air interface part of the incident electric field is reflected back to the prism with coefficient ρ_1 and angle θ_1. Also, part of the field is transmitted from the prism to the resonator, with coefficient τ_{12} and angle θ_2 (see Fig. 2(a)). Similarly, after one round-trip of the circulating WGM, the field is incident from the resonator with angle θ_2, being part of it transmitted back to the prism with coefficient τ_{21} and angle θ_1, and another part reflected inside the resonator with coefficient ρ_2 and angle θ_2 (see Fig. 2(b)). Invoking the reciprocity theorem with the fields described in both situations shown in Fig. 2 such that $\oint_S E_a \times H_b \cdot \mathrm{d}S = \oint_S E_b \times H_a \cdot \mathrm{d}S$ where the surface S is a box with two of their faces parallel to the interfaces, it can be shown that for nonmagnetic media

Optics EXPRESS

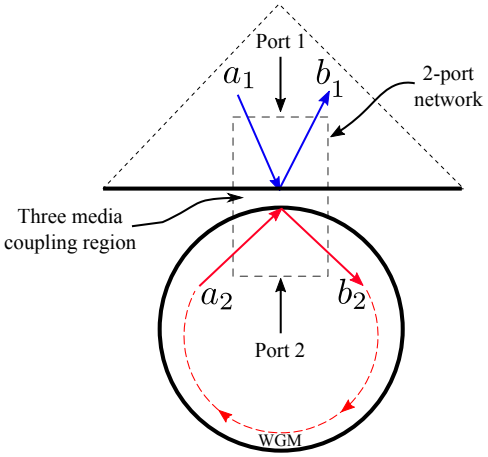

Fig. 3. Two-port network scheme.

$$\tau_{21} = \frac{n_2}{n_1}\frac{\cos\theta_2}{\cos\theta_1}\tau_{12} \tag{3}$$

Additionally, merging both scenarios shown in Fig. 2, the power conservation principle can be applied such that

$$\frac{\left|E_{1a}^{+}\right|^2 - \left|E_{1a}^{-} + E_{1b}^{+}\right|^2}{\left|E_{2a}^{+} + E_{2b}^{-}\right|^2 - \left|E_{2b}^{+}\right|^2} = \frac{n_2\cos\theta_2}{n_1\cos\theta_1}, \tag{4}$$

leading to the relation

$$\rho_2 = -\frac{\tau_{12}}{\tau_{12}^*}\rho_1^* \tag{5}$$

The mathematical expressions relating ρ_1 and τ_{12} to n_1, n_2, h and θ_1, are not necessary by now. However, the function ρ_1 will be explicitly calculated later in this paper. Following an analog procedure, the above equations can be derived for electric fields polarized parallel to the plane of incidence.

3. Coupling optimization

The whole coupling situation described above can be viewed as a two-port network where the ports are the prism and the resonator media, each one supporting an incident and a reflected wave as shown in Fig. 3, whose electric fields are related as

$$\begin{bmatrix} E_1^- \\ E_2^- \end{bmatrix} = \begin{bmatrix} \rho_1 & \tau_{21} \\ \tau_{12} & \rho_2 \end{bmatrix}\begin{bmatrix} E_1^+ \\ E_2^+ \end{bmatrix} \tag{6}$$

Defining the power waves as $a_i = \sqrt{\frac{n_i\cos\theta_i}{2\eta_0}}E_i^+$ and $b_i = \sqrt{\frac{n_i\cos\theta_i}{2\eta_0}}E_i^-$ where $\eta_0 = \sqrt{\frac{\mu_0}{\varepsilon_0}}$, then $|a_i|^2$ and $|b_i|^2$, $i = 1, 2$ gives the incident and reflected power respectively in the corresponding port (strictly speaking, they represent the power by unit area on the interfaces surfaces). From this and Eq. (3), Eq. (6) can be rewritten as

$$\begin{bmatrix} b_1 \\ b_2 \end{bmatrix} = \begin{bmatrix} \rho_1 & k \\ k & \rho_2 \end{bmatrix}\begin{bmatrix} a_1 \\ a_2 \end{bmatrix}, \tag{7}$$

Optics EXPRESS

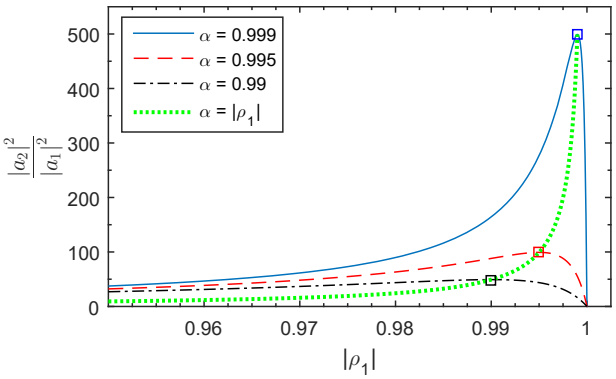

Fig. 4. WGM power relative to incident laser power versus $|\rho_1|$ for three different values of α. Note that the maximum intracavity power (critical coupling) is achieved at the marked positions corresponding to $\alpha = |\rho_1|$.

where $k = \tau_{12}\sqrt{\frac{n_2 \cos\theta_1}{n_1 \cos\theta_2}} = |k|\, e^{j\varphi}$, $\rho_1 = |\rho_1|\, e^{j\beta_1}$ and $\rho_2 = |\rho_1|\, e^{j\beta_2}$. The field after one round-trip of the WGM E_2^+ can be related with E_2^- by considering a phase shift ξ and an attenuation factor $0 \leq \alpha \leq 1$ given by the losses in the resonator, such that $\alpha = 1$ for a lossless WGM propagation. Hence,

$$a_2 = \alpha e^{j\xi} b_2 \tag{8}$$

The WGM is in resonance if $\xi + \beta_2 = 2\pi m, m = \pm 1, \pm 2, \ldots$, i.e., when the field adds constructively with itself after being reflected at the coupling point inside the resonator. Substituting Eq. (8) into Eq. (7) considering the resonance condition, the reflected power in each medium results

$$|b_1|^2 = \frac{(\alpha - |\rho_1|)^2}{(1 - \alpha\,|\rho_1|)^2}\,|a_1|^2 \tag{9}$$

$$|b_2|^2 = \frac{1 - |\rho_1|^2}{(1 - \alpha\,|\rho_1|)^2}\,|a_1|^2 \tag{10}$$

where we have used $|k|^2 = 1 - |\rho_1|^2$, which can be demonstrated by using the power conservation principle $|a_1|^2 + |a_2|^2 = |b_1|^2 + |b_2|^2$ along with Eq. (5). By differentiating with respect to $|\rho_1|$, it is found that $|b_2|^2$ (and $|a_2|^2$) have an absolute maximum when $|\rho_1| = \alpha$ as can be noted in Fig 4 which agrees with [15]. This is called critical coupling and is the desired working point because the highest possible level of power is circulating inside the resonator. This point coincides with impedance matching since no power is reflected back to the prism ($|b_1|^2 = 0$) and all the laser power is coupled into the resonator, continuously increasing the field inside to the highest level due to constructive interference. This occurs until the steady-state is reached where the incoming laser power compensates radiation and intrinsic losses in the resonator medium. Figure 4 also shows the WGM power to incident laser power ratio when critical coupling is enforced. For $\alpha > 1/\sqrt{2}$ the power circulating inside the resonator is higher than the incoming laser power. This power enhancement defines the Finesse of the resonator $\mathcal{F} = \frac{|a_2|^2}{|a_1|^2}$ and may reach considerably high levels for low losses.

Optics EXPRESS

4. Tuning for critical coupling

Applying boundary conditions, we can derive the Fresnel's coefficients for the problem in Fig. 2(a) to obtain the reflection coefficient ρ_1, which results in

$$\rho_1 = \frac{n_1 \cos\theta_1(1+r) - C_0(1-r)}{n_1 \cos\theta_1(1+r) + C_0(1-r)}, \tag{11}$$

where,

$$r = \frac{C_0 - n_2 C_2}{C_0 + n_2 C_2} e^{-j\frac{4\pi}{\lambda_0} h C_0}, \tag{12}$$

$$C_0 = j\sqrt{n_1^2 \sin^2\theta_1 - 1} \tag{13}$$

$$C_2 = \sqrt{1 - \left(\frac{n_1}{n_2}\right)^2 \sin^2\theta_1}, \tag{14}$$

and λ_0 is the wavelength of light in the air gap. For a given incidence angle θ_1, which is conditioned by Eq. (2), the value of $|\rho_1|$ can be tuned for critical coupling by changing the air gap thickness h. The dependence of $|\rho_1|$ with h can be introduced in Eqs. (8) and (10) to obtain the finesse as a function of h. This is plotted for a given α, and three different incidence angles in Fig. 5. Note the sub-wavelength available range for tuning the thickness h. For instance, with $\lambda_0 = 1550$ nm, a resolution of h on the order of tens of nanometers is needed. This range scales with the decay length of the evanescent field which decreases with the incidence angle. For a given value of losses α, we can calculate the required distance h to reach critical coupling for a given incidence angle θ_1 as shown in Fig. 6.

5. Resonator geometry optimization

The actual surface of the resonator at the coupling region is not flat. This has to be taken into consideration since the air gap h is now variable below the projection of the laser beam on the prism interface. Asuming a Gaussian beam is incident on the first prism face with angle α_0 as shown in Fig. 7, the refracted beam with angle α_1 according to Snell's laws, will have an elliptical transversal section with semi-major over semi-minor axis ratio $\cos\alpha_1/\cos\alpha_0$. Then, defining $\Delta\beta = \theta_1 - \beta = \alpha_1$ where β is the angle of the prism, the beam's footprint at the interface $z = 0$ is an ellipse which field is described by

$$\Psi_1(x,y) = e^{-\frac{1}{W^2}(x^2 + (y\cos\theta_1 b(\Delta\beta))^2)}, \tag{15}$$

with,

$$b(\Delta\beta) = \frac{\sqrt{1 - n_1^2 \sin(\Delta\beta)^2}}{\cos\Delta\beta} \tag{16}$$

where W is the beam's waist size. The parameter $b(\Delta\beta)$ describes the elliptical deformation of the beam when refracted in the prism due to the difference between the required incidence angle θ_1 and the angle of the prism β. Hence, the iso-scalar curves of the footprint at $z = 0$ are ellipses with semi-minor over semi-major axes ratio equal to $\cos\theta_1 b(\Delta\beta)$. If critical coupling is desired,

Optics EXPRESS

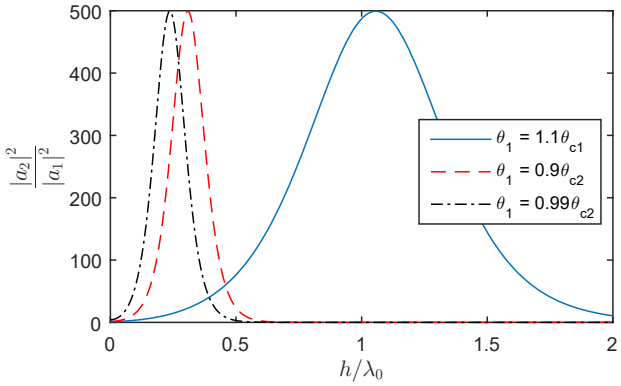

Fig. 5. Power enhancement as a function of h for three different incidence angles greater than the critical angle between prism and air $\theta_{c1} = \arcsin(1/n_1)$ (evanescent field is generated), and less than the critical angle between prism and resonator $\theta_{c2} = \arcsin(n_2/n_1)$ (to avoid total internal reflection in the whole system). For this particular example, the prism is made of diamond ($n_1 = 2.39$) and the resonator is made of $LiNbO_3$ ($n_2 = 2.21$). The absorption coefficient of $LiNbO_3$ is about $\kappa'' = 5 \times 10^{-2}$, so for a resonator with radius $R_0 = 2.5$mm, $\alpha \approx e^{-2\pi\kappa'' R_0} = 0.999$.

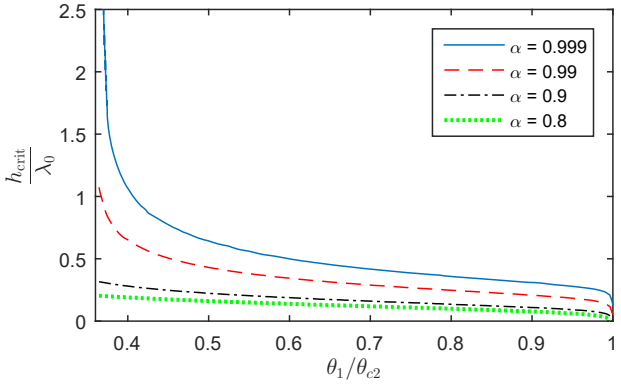

Fig. 6. Optimal h as a function of θ_1/θ_{c2} for four different values of α. The media considered are the ones of Fig. 5. $\theta_{c2} = \arcsin(n_2/n_1)$ is the critical angle between prism and resonator. In real resonators, however, angles close to θ_{c2} cannot be used due to the finite coupling length of the curved surface and the plane prism interface which will be shown in Section 5.

no reflected field must exist at the prism-air interface. Therefore, the evanescent WGM field scattered back to the prism must interfere destructively with the natural reflection of the incident beam at the prism-air interface, which means that they must have the same spatial distribution. From uniqueness theorem, the foregoing implies that the field in the air gap must match the footprint distribution of Eq. (15) when evaluated at the prism interface. As an approximation, we will consider the evanescent WGM field as a primary field in the air gap. For axisymmetric resonators as the one shown in Fig. 8 with curvature radii R_0 and r_0, the field distribution at the rim surface has the approximated form [16]

$$E|_{r=r_0} \propto e^{-\gamma^2/2\gamma_m^2} e^{-jm\varphi} \tag{17}$$

Optics EXPRESS

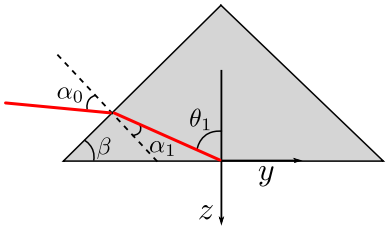

Fig. 7. Gaussian beam refraction.

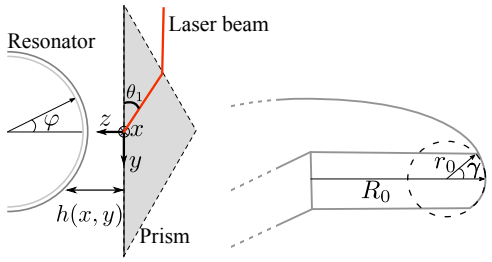

Fig. 8. Left: Resonator-prism configuration. Right: Disc-shaped WGM resonator geometry.

where φ is the equatorial angle of the resonator, m is the mode number of the WGM, γ is the elevation angle shown in Fig. 8, and $\gamma_m = \frac{1}{\sqrt{m}}\left(\frac{R_0}{r_0}\right)^{3/4}$. Eq. (17) is valid for high mode number m, in which case the evanescent field outside the resonator decreases from the rim with the dependence [13]

$$E_e \propto E|_{r=r_0}\, e^{-\kappa''(r-r_0)} \tag{18}$$

with $\kappa'' = \frac{2\pi}{\lambda_0}\sqrt{n_2^2 - 1}$. According to Fig. 8, at the coupling region $(x, y) \approx (0, 0)$, so the angles φ and γ are small. In this case $r|_{z=0} - r_0 \approx h$, being $h = (x, y)$ the variable distance between prism and resonator which can be obtained from geometrical relations as

$$h = d + R_0 - r_0\sqrt{\left(\frac{R_0}{r_0} - 1 + \sqrt{1 - \left(\frac{x}{r_0}\right)^2}\right)^2 - \left(\frac{y}{r_0}\right)^2} \tag{19}$$

where d is the shortest distance between prism and resonator. In the vicinity of the coupling region, $x \ll r_0$ and $y \ll r_0$, thereby $\sqrt{1-(x/r_0)^2} \approx 1 - \frac{1}{2}(x/r_0)^2$ and $(x/r_0)^4 \ll (x/r_0)^2, (y/r_0)^2$. This results in the expression

$$h \approx d + R_0 - R_0\sqrt{1 - \frac{1}{R_0}\left[\left(\frac{x}{\sqrt{r_0}}\right)^2 + \left(\frac{y}{\sqrt{R_0}}\right)^2\right]} \tag{20}$$

Eq. (20) shows that h is constant over concentric ellipses with semi-minor over semi-major axes ratio equal to $\sqrt{r_0/R_0}$. This equation can be simplified further by taking again the first two terms of the binomial series of the square root, yielding

$$h(x, y) \approx r|_{z=0} - r_0 \approx d + \frac{1}{2}\left[\left(\frac{x}{\sqrt{r_0}}\right)^2 + \left(\frac{y}{\sqrt{R_0}}\right)^2\right] \tag{21}$$

Optics EXPRESS

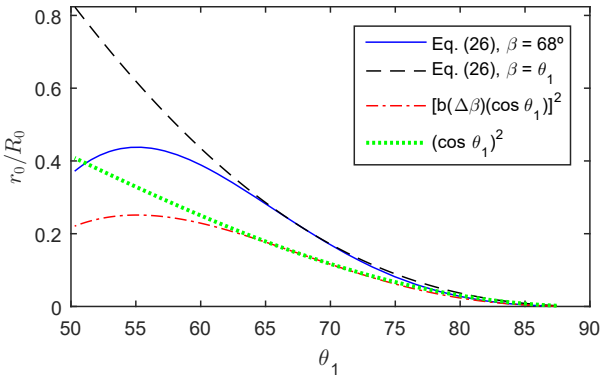

Fig. 9. Optimal ratio r_0/R_0 of a $LiNbO_3$ resonator as a function of the incidence angle θ_1 calculated by neglecting the dependence of the WGM with γ and by Eq. (26) for the cases of $\beta = \theta_1$ and $\beta = 68°$ which is the required incidence angle for a diamond prism and a $LiNbO_3$ resonator.

Substituting Eq. (21) in Eq. (18), and approximating $\gamma \approx \sin\gamma = x/r_0$, we get the evanescent field of the WGM at the prism plane

$$E_e|_{z=0} \propto e^{-\frac{1}{2}\left[(x/\Delta x)^2+(y/\Delta y)^2\right]} e^{-jm\varphi} \tag{22}$$

with,

$$\Delta x^2 = \frac{r_0^2\gamma_m^2}{1+\kappa'' r_0\gamma_m^2} \tag{23}$$

and,

$$\Delta y^2 = \frac{R_0}{\kappa''} \tag{24}$$

Since we are interested in the spatial distribution of the evanescent WGM field at the prism, the phase term of Eq. (22) is ignored as the phase matching in y direction is already considered in Eq. (2). In order to match the elliptical field distribution of Eq. (22) with the one of the footprint of the incoming laser beam given in Eq. (15),

$$[b(\Delta\beta)\cos\theta_1]^2 = \frac{\Delta x^2}{\Delta y^2} = \frac{r_0}{R_0}\left(\frac{\kappa'' r_0\gamma_m^2}{1+\kappa'' r_0\gamma_m^2}\right) \tag{25}$$

If the dependence with γ of the WGM field distribution in Eq. (17) is neglected, then $\gamma_m \to \infty$ and $\cos\theta_1 \approx \sqrt{\frac{r_0}{R_0}}$ as reported in [17]. However, by writing $m \approx \frac{\omega}{c} n_2 R_0$ (the mode number represents the number of wavelengths fitting along the perimeter of the resonator), Eq. (25) can be rewritten as

$$[b(\Delta\beta)\cos\theta_1]^2 \approx \frac{r_0}{R_0}\left(1+\frac{n_2}{\sqrt{n_2^2-1}}\sqrt{\frac{r_0}{R_0}}\right)^{-1} \tag{26}$$

where the second term in the parentheses is in general not negligible. For a $LiNbO_3$ resonator and a diamond prism with $\beta = \theta_1$, the error in the optimal ratio r_0/R_0 calculated by neglecting the dependence of the WGM with γ, with respect to an optimal ratio calculated from Eq. (26) is about 30%. For a fixed prism angle $\beta = 68°$, the optimal ratio r_0/R_0 is obtained for different

Optics EXPRESS

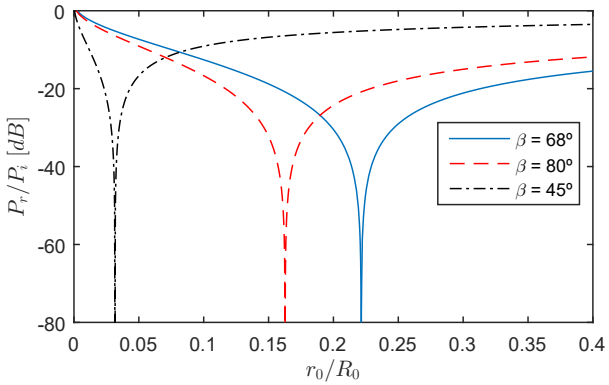

Fig. 10. Reflected beam's normalized power as a function of the ratio r_0/R_0 for three different prism angles and $\theta_1 = 68°$.

values of θ_1 and compared with the case of normal incidence on the prism face ($\beta = \theta_1$) as depicted in Fig. 9. As expected, the curves overlap at $\theta_1 = 68°$ and the difference between them is less than 1% withing a θ_1 range of about 5 degrees. The normalized reflected beam power can be calculated by taking the contribution of the WGM field refracted to the prism which destructively interferes with the naturally reflected beam at the pirsm-air interface at critical coupling, yielding

$$\frac{P_r}{P_i} = 1 + 2b\cos(\theta_1)\frac{\Delta x \Delta y}{W^2} - 8b\frac{\Delta x \Delta y}{\sqrt{(2\Delta x^2 + W^2)(2b^2\Delta y^2 + W^2)}} \tag{27}$$

Figure 10 shows the normalized reflected power as a function of the geometry of the resonator r_0/R_0 for a fixed $\theta_1 = 68°$, a beam focused such that the footprint matches in the x direction with the WGM field of Eq. (22) and different prism angles β. The reflected beam is totally canceled for the ratio given by Eq. (26) in each case, whereas by using the simplified version of Eq. (26) considering $\gamma_m \to \infty$, the normalized reflected power is larger than -20 dB. As it may be noticed, the system is more tolerant to errors in r_0/R_0 dimensions for normal incidence with the prism's face ($\beta = \theta_1$) in which case the ratio is maximum. Since $b(\Delta\beta)$ is an even function of $\Delta\beta$, the ratio will decrease for any mismatch between θ_1 and β.

It is important to mention that in practice the footprint of the laser and the Gaussian window of Eq. (22) do not have exactly the same dimensions since the laser beam is not perfectly focused to have the required beam waist size. Therefore, total destructive interference does not occur and a partially reflected beam at the prism can be observed even under critical coupling. This explains why experimentally in the setup of Fig. 1 the laser pump is always visible in the optical spectrum analyzer along with the generated sidebands [17].

6. Conclusion

The conditions required for achieving the optimal coupling of a laser beam into a WGM resonator have been discussed. With optimal coupling, the maximum possible level of power circulates within the resonator, being this orders of magnitude larger than the incoming laser pump depending on the resonator losses. The conditions required to achieve it can be summarized as follows:

- Given the n_{eff} of the WGM and the media electromagnetic characteristics n_1, n_2, an incidence angle θ_1 must be chosen according to Eq. (2)

Optics EXPRESS

- Given the coupling angle θ_1, the geometry of the rim is chosen according to Eq. (26).
- Finally, the distance d is tuned to accomplish the critical coupling condition. This gap can be found approximately from the curves of Fig. 6.

Consequently, the shape of the resonator is determined by the refractive index of the media and the operation frequency. It can be shown that the Finesse of a critically coupled resonator increases with the Q factor and scales inversely with the mode number m. The absorption Q factor is fixed by the material properties and the radiation Q factor grows very quickly with m. Therefore, in the THz domain, for a given frequency it is desired to have tiny resonators so the number of wavelengths in the azimuthal direction m is small, provided that radiation losses are negligible with respect to absorption losses and the Q factor is not degraded by the radiation of the mode. For example, for a Lithium Niobate resonator at sub-THz frequencies, the total Q factor is determined by the absorption quality factor which is about $Q_{\mathrm{abs}} \approx 280$ for $m \geq 4$. Thus, the mode $m = 4$ optimizes the critically-coupled finesse of the resonator. The coupling of low-frequency fields into WGM resonators still needs to be analytically studied in order to be optimized.

Acknowledgment

This work has been financially supported by “DiDaCTIC: Desarrollo de un sistema de comunicaciones inalámbrico en rango THz integrado de alta tasa de datos”, TEC2013-47753-C3, CAM S2013/ICE-3004 “DIFRAGEOS” projects, “Proyecto realizado con la Ayuda Fundación BBVA a Investigadores y Creadores Culturales 2016.” and “Estancias de movilidad de profesores PRX16/00021”.